ResearchGate

See discussions, stats, and author profiles for this publication at: https://www.researchgate.net/publication/339670097

Fabrication and Analysis of the Current Transport Mechanism of Ni/n-GaN Schottky Barrier Diodes through Different Models

Article *in* Semiconductors · February 2020

DOI: 10.1134/S1063782620020141

CITATIONS
3

READS
37

3 authors:

Santosh Kumar
University of Mysore

4 PUBLICATIONS **3** CITATIONS

SEE PROFILE

VINAY KUMAR M
K.L.E. Society's Raja Lakhamagouda Science Institute

12 PUBLICATIONS **12** CITATIONS

SEE PROFILE

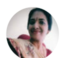

Krishnaveni S
University of Mysore

39 PUBLICATIONS **460** CITATIONS

SEE PROFILE

Some of the authors of this publication are also working on these related projects:

Nanogenerators View project

FLEXIBLE TRIBOELECRTIC NANOGENERATOR View project

All content following this page was uploaded by VINAY KUMAR M on 04 March 2020.

The user has requested enhancement of the downloaded file.

ISSN 1063-7826, Semiconductors, 2020, Vol. 54, No. 2, pp. 169–175. © Pleiades Publishing, Ltd., 2020.

ELECTRONIC PROPERTIES OF SEMICONDUCTORS

Fabrication and Analysis of the Current Transport Mechanism of Ni/*n*-GaN Schottky Barrier Diodes through Different Models

S. Kumar[a], M. V. Kumar[b], and S. Krishnaveni[a],*

[a] *Department of Studies in Physics, Manasagangotri, University of Mysore, Mysuru, 570006 India*

[b] *Department of Physics, K.L.E Society's R.L.S Institute, Belagavi, 590001 India*

**e-mail: sk@physics.uni-mysore.ac.in*

Received May 15, 2019; revised October 9, 2019; accepted October 9, 2019

Abstract—The current transport mechanism of indigenously fabricated Ni/*n*-GaN Schottky barrier diodes (SBDs) has been analysed using the current–voltage (*I–V*) and capacitance–voltage (*C–V*) measurements. Various models like Rhoderick's method, Cheung's method, Norde's method, modified Norde's method, Hernandez's method, and Chattopadhyay's method have been used to extract the different electric parameters from the *I–V* curve. A comparison has been made between the various electrical parameters such as ideality factor, barrier height, and series resistance, which are extracted from the forward bias *I–V* curve of Ni/*n*-GaN SBDs. The carrier concentration of the substrate and the barrier height is obtained from *C–V* characteristics of Ni/*n*-GaN SBDs. We observe from the reverse current characteristics that the Ni/*n*-GaN SBDs show the dominance of Schottky emission in intermediate and higher voltages.

Keywords: Schottky contacts, GaN, electrical properties, Rhoderick's method, Cheung's method, Norde's method, Modified Norde's method, Hernandez's method, Chattopadhyay's method, current transport mechanism

DOI: 10.1134/S1063782620020141

1. INTRODUCTION

Wide-bandgap semiconductors (WBGSs) like gallium nitride (GaN), aluminum nitride (AlN) etc. are being extensively used in the modern electronic device fabrication technology. For modern electronic devices, GaN is the potential material having exceptional properties like direct band gap, high chemical resistance, high melting point, and good thermal conductivity [1–7]. Metal–semiconductor (M–S) contacts are an essential aspect of electronic devices, and optimization of electronic properties of GaN-based devices requires the elaboration of stable and reliable ohmic and Schottky contacts. Current–Voltage (*I–V*) and Capacitance–Voltage (*C–V*) characteristics of the M–S interface give enormous depths of information on the physical and electrical properties of a bulk semiconductor material and its interface. Therefore, the analysis of electrical parameters with different methods leads to a better understanding of the current transport mechanism which is highly essential for device fabrication technology.

The studies on extraction of electrical parameters by different methods like Rhoderick's method [8], Cheung's method [9], Norde's method and Modified Norde's method [10, 11], Hernandez's method [12], and Chattopadhyay's method [13] are very essential and helpful in better understanding the electrical properties of M–S Schottky interfaces. Further, the analysis of reverse *I–V* characteristics will reveal the conduction mechanism of M–S Schottky contacts [14–20]. Usually, the electrical parameters extracted from *I–V* characteristics are affected by image-force effects, dipole lowering effects, tunneling currents, and leakage currents [21–25]. Whereas, *C–V* characteristics give more veracious results of electrical parameters [26–30].

In the present study, we report the fabrication of Ni/*n*-GaN Schottky barrier diodes (SBDs). Analysis of its current transport mechanism by *I–V* characteristics has been analyzed through various models and the comparative study has been done for extracted electrical parameters.

2. EXPERIMENTAL

The Si-doped GaN (0001) on sapphire (0001) wafers of thickness 4 μm having dimensions of 10 × 5 mm are used for the fabrication of GaN SBDs. Before deposition of ohmic contacts, wafers of *n*-GaN were cleaned in different steps as: boiling in aqua regia for removing the native surface contamination, cleaning in deionised water, degreasing the wafers by boiling in trichloroethylene, rinsing in boiled isopropanol, rinsing in deionised water, and finally dipped into a

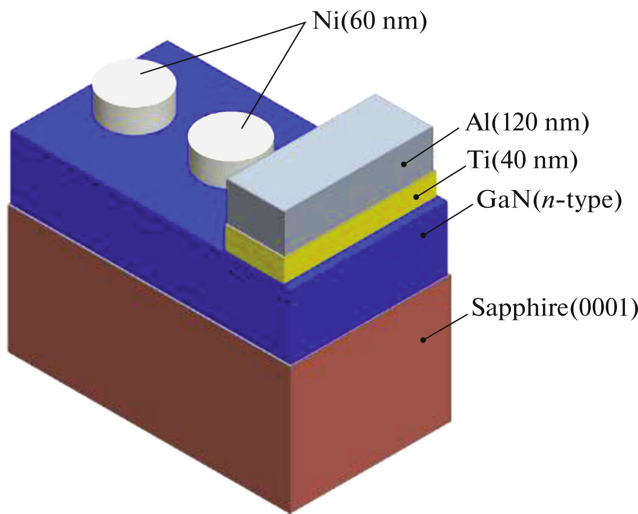

Fig. 1. Structure of Ni/n-GaN SBDs.

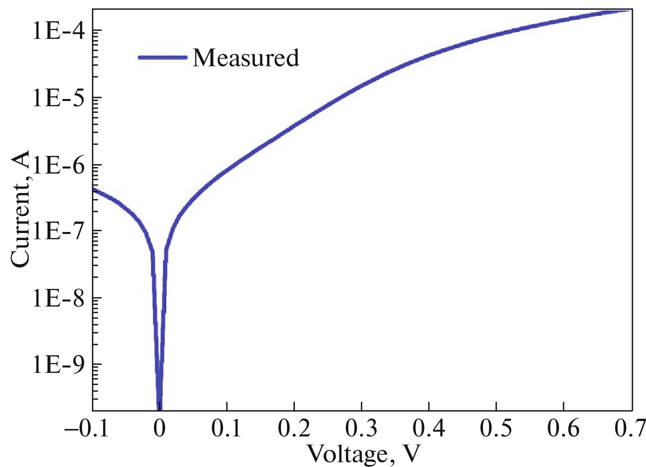

Fig. 2. The plot of I–V characteristics for Ni/n-GaN SBDs.

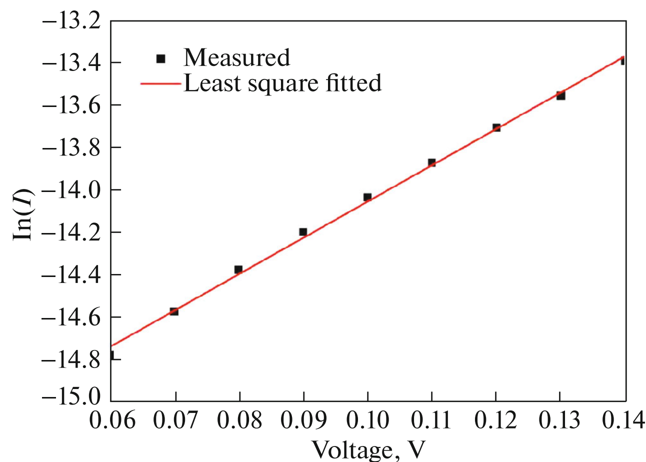

Fig. 3. The plot of ln(I) vs. voltage for Ni/n-GaN SBDs.

solution with equal ratio of HCl and H_2O for 10 s. After wafer cleaning, the layers of ohmic contacts were deposited by evaporating titanium|aluminum (Ti|Al, 40|120 nm) using an electron beam (e-beam) evaporation system at a pressure of 6×10^{-9} bar. Finally, using an e-beam evaporation system at a pressure of 6×10^{-9} bar, Schottky contacts were deposited by evaporating nickel (Ni, 60 nm) by using a stainless-steel mask in contact with the n-GaN (Fig. 1). I–V and C–V characterization of Ni/n-GaN SBDs were performed at room temperature using semiconductor device parameter analyzer (Agilent Technologies B1500A).

3. RESULTS

3.1. Current–Voltage (I–V) Characteristics

The transport mechanism of the Schottky junction is governed by the thermionic emission of majority carriers over the potential barrier that forms at the M–S interface. The current due to thermionic emission for an applied voltage is given by [8]:

$$I = I_0 \exp\left(\frac{qV}{nkT}\right)\left[1 - \exp\left(-\frac{qV}{nkT}\right)\right], \quad (1)$$

where the symbols have their usual conventional meanings.

Figure 2 represents the I–V characteristics of Ni/n-GaN SBDs. According to Rhoderick's method, the ideality factor n and the barrier height φ_B are given by the slope and the intercept of the plot of ln$I$ vs. voltage (Fig. 3), respectively.

The values of the ideality factor n, saturation current I_0, and barrier height φ_B were determined to be 2.25, 3.56×10^{-8} A, 0.698 eV, respectively. For low-resistance diode, this method holds good since low resistance is ignored for low forward-bias voltage [9, 10]. From Fig. 2, it appears that Ni/n-GaN SBDs in the present study do not have low resistance.

The series resistance R_S is an essential parameter of M–S contacts, which affects the electrical properties of SBDs. The SBDs parameters like Schottky barrier height B, ideality factor n, and series resistance R_S can also be obtained using Cheung and Cheung's method [9]. According to [9], the thermionic emission I–V characteristics of SBDs with series resistance R_S can be expressed as

$$I = I_0 \exp\left(-\frac{q(V - IR_S)}{nkT}\right), \quad (2)$$

where the IR_S is the voltage drop across R_S of SBDs. Cheung's functions can be written as follows

$$\frac{dV}{d(\ln I)} = IR_S + n\left[\frac{kT}{q}\right], \quad (3)$$

$$H(I) = V + n\frac{kT}{q}\ln\left[\frac{I}{AA^{*}T^{2}}\right], \quad (4)$$

$$H(I) = n\varphi_{B} + IR_{S}. \quad (5)$$

The value of n is 1.14, and the value of R_S is 55.98 kΩ from Fig. 4.

Another value of R_S is given by the slope of the plot of Fig. 5.

These two values of series resistance R_S prove the validity of Cheung's method. The values of R_S obtained from these two plots are nearly going on par with each other which gives the uniformity of Cheung's method. By this method, the average value of R_S is 60.88 kΩ, and the value of φ_B is 0.687 eV.

For the diodes with large series resistance, Norde [10, 11] developed a method to determine φ_B and R_S. Usually, the values of n lie between 1 and 2, so to determine large values of R_S of diodes, the modified Norde's method is used. Norde's method involved the function $F(V)$ given as

$$F(V) = \frac{V}{2} - \frac{kT}{q}\ln\left(\frac{I(V)}{AA^{*}T^{2}}\right). \quad (6)$$

The current I_0 corresponding to minima of $F(V)$ vs. V plot will give R_S as

$$R_{S} = \frac{kT}{qI_{0}}, \quad (7)$$

and φ_B is given as

$$\varphi_{B} = F(V_{0}) + \frac{V_{0}}{2} - \frac{kT}{q}, \quad (8)$$

where $F(V_0)$ and V_0 are the values of $F(V)$ and V corresponding to the least value of current I_0. In modified Norde's method, $F(V)$ is defined as

$$F(V) = \frac{V}{\gamma} - \frac{kT}{q}\ln\left(\frac{I(V)}{AA^{*}T^{2}}\right). \quad (9)$$

Since the ideality factor lies between 1 and 2, therefore, $\gamma = 2$ (>1). The R_S and φ_B can be calculated using the following equations:

$$R_{S} = \frac{kT(\gamma - 1)}{qI_{0}}, \quad (10)$$

$$\varphi_{B} = F(V_{0}) + \frac{V_{0}}{\gamma} - \frac{kT}{q}. \quad (11)$$

From the plot of $F(V)$ vs. voltage (Fig. 6), the value of R_S is 45.47 kΩ, and φ_B is 0.687 eV.

Another method that accounts for the voltage-dependent nature of the ideality factor (n), the barrier height φ_B and the series resistance R_S was developed by

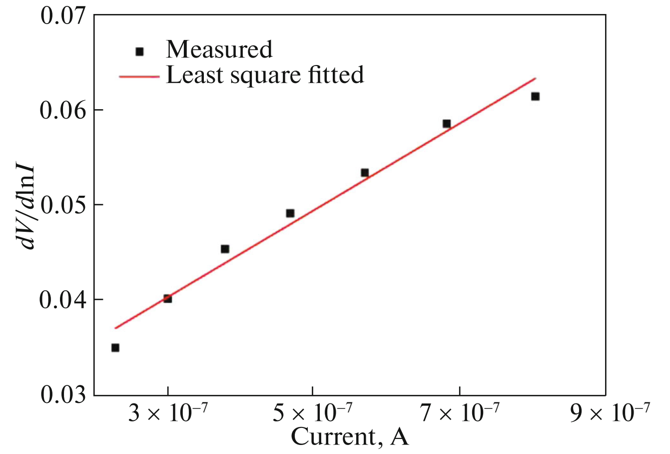

Fig. 4. The plot of $dV/d\ln(I)$ vs. current for Ni/n-GaN SBDs.

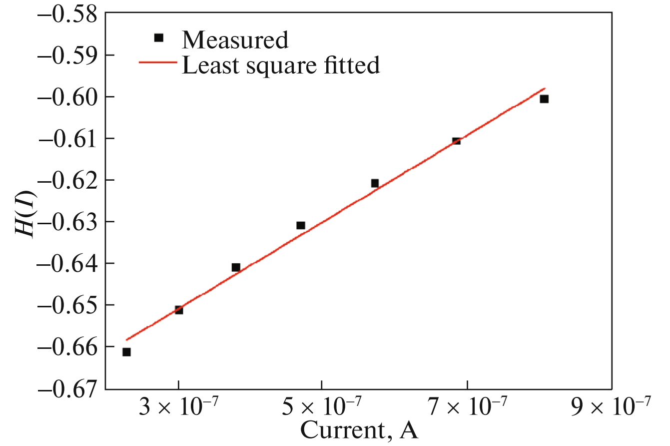

Fig. 5. The plot of $H(I)$ vs. I for Ni/n-GaN SBDs.

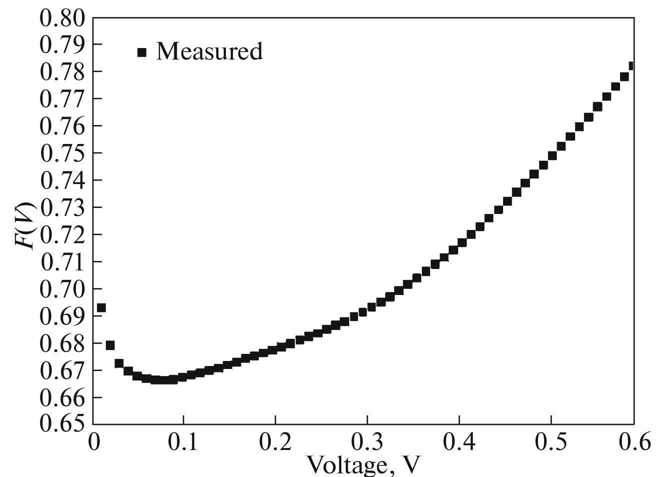

Fig. 6. The plot of $F(V)$ vs. voltage for Ni/n-GaN SBDs.

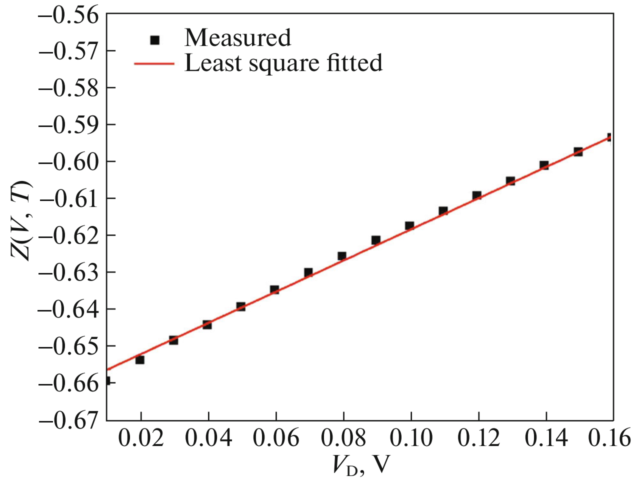

Fig. 7. The plot of $Z(V, T)$ vs. V_D for Ni/n-GaN SBDs.

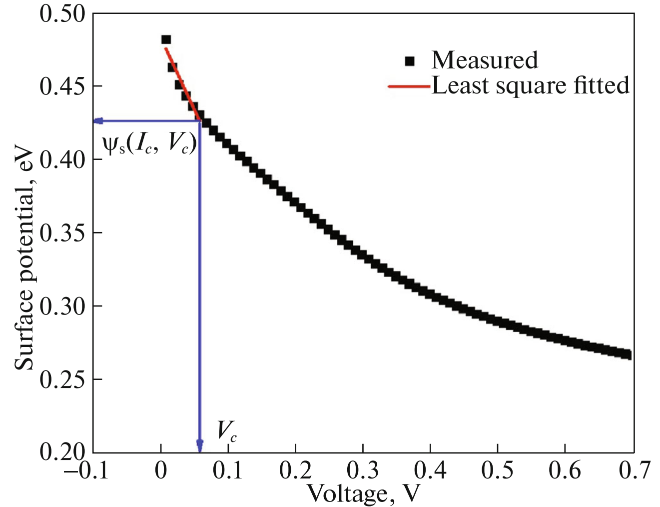

Fig. 8. The plot of Surface potential vs. V for Ni/n-GaN SBDs.

Hernandez et al. [12]. They have formulated a voltage-dependent function $Z(V, T)$ given as

$$Z(V,T) = \frac{kT}{q}\ln\left(\frac{1}{AA^*T^2\left[1-\exp\left(-\frac{qV_D}{kT}\right)\right]}\right), \quad (12)$$

$$Z(V,T) = -\varphi_B(V,T) + \frac{V_D}{n_0(V,T)}. \quad (13)$$

From Fig. 7, the values of voltage-dependent ideality factor n and the barrier height φ_B obtained are 2.18 and 0.667 eV, respectively.

For large values of R_S, the ln$I$ vs. V plot become non-linear. This leads to a severe problem in finding the saturation current. Hence, the extracted values of φ_B are not reliable. Chattopadhyay developed a model [13] to account for this problem and defined the surface potential Ψ_S which is given as

$$\Psi_S = \frac{kT}{q}\ln\left(\frac{AA^*T^2}{I}\right) - V_n, \quad (14)$$

φ_B and n can be written as [14, 15]

$$\varphi_B = \Psi_S(I_C, V_C) + C_2V_C + V_n, \quad (15)$$

$$C_2 = \frac{1}{n} = -\left(\frac{d\Psi_S}{dV}\right)_{I_C,V_C}. \quad (16)$$

From Fig. 8, the values of V_C and $\Psi_S(I_C, V_C)$ obtained are 0.06 and 0.43 eV, respectively. From Eqs. (15) and (16), the calculated values of φ_B and n are 0.657 eV and 1.04, respectively.

Tables 1 and 2 list the extracted values of ideality factor n, series resistance R_S, and barrier height φ_B from the different methods.

The value of ideality factor n is found to vary from 1.04 to 2.25 in different methods, which shows non-ideal I–V behaviour. The value of barrier height φ_B is found to vary from 0.657 to 0.698 eV from the above methods, which is low in comparison to the value observed in the case of Ni/n-GaN SBDs [16–20].

Table 1. The values of ideality factor n of Ni/n-GaN SBDs extracted from Rhoderick's method, Cheung's method, Hernandez's method, and Chattopadhyay's method

$n(I–V)$	$n(dV)/d(\ln I)$	$n(Z–V)$	$n(\Psi_S–V)$
2.25	1.14	2.18	1.04

Table 2. The values of series resistance (R_S) and barrier height (φ_B) of Ni/n-GaN SBD's extracted from the Cheung's method, Norde's method (NM), modified Norde's method (MNM), Hernandez's method, and Chattopadhyay's method

Barrier height φB, eV					Series resistance RS, kΩ			
$I–V$	$H(I)$	$F(V)$	$Z-V$	$\Psi_S–V$	$dV/d\ln I$	$H(I)$	$F(V)$(NM)	$F(V)$(MNM)
0.698	0.687	0.681	0.667	0.657	55.98	65.77	45.32	43.42

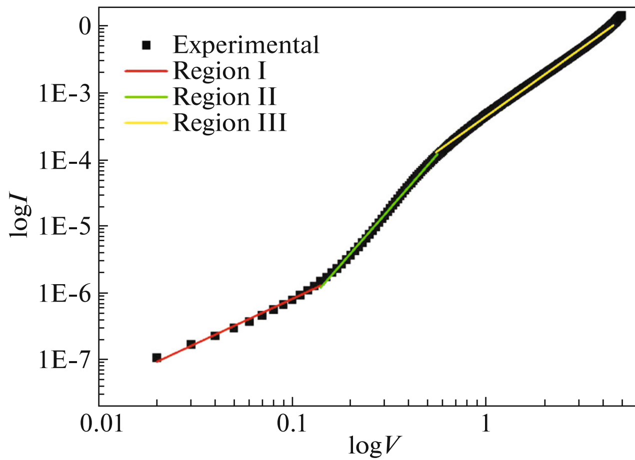

Fig. 9. The plot of log*I* vs. logV for Ni/*n*-GaN SBDs.

The log*I* vs. log*V* plot (Fig. 9) is analysed to study the dominance of the current conduction mechanism in the forward-bias region of *I*–*V* characteristics.

The existence of different current conduction mechanisms can be shown in the log*I* vs. log*V* plot, which has different linear regions (I, II, and III) with different slopes. In Region I, the value of slope is 1.35 close to unity, which indicates an ohmic behaviour, which may be due to the "background doping" or "thermally generated carriers" [12, 17]. The value of slope is 3.31 in Region II, higher than 2.0, and this may be due to the "space-charge-limited current (SCLC)" with "discrete trapping levels". For Region III, the slope value decreases to 2.08, since the Ni/*n*-GaN SBDs may reach the "trap-filling" limit [18, 19].

Figure 10 shows the variation of reverse current (I_R) with reverse voltage, indicates that either the Poole–Frenkel emission (PFE) or Schottky emission (SE) mechanisms are dominant in the M–S junction.

The current through the diode for PFE [20] and SE [21] are given by

$$I_R \propto E \exp\left(\frac{1}{kT}\right)\sqrt{\frac{qE}{\pi\varepsilon_0\varepsilon_r}}, \quad (17)$$

$$I_R \propto T^2 \exp\left(\frac{1}{2kT}\right)\sqrt{\frac{qE}{\pi\varepsilon_0\varepsilon_r}}. \quad (18)$$

From Fig. 10, the slopes of plots can be expressed as [22, 23]

$$S = \frac{1}{nkT}\sqrt{\frac{q}{\pi\varepsilon_0\varepsilon_r}}. \quad (19)$$

The value of n is 1 for PFE, and the value of n is 2 for SE. The theoretical values of the slopes of plots are given in Table 3. The slopes obtained from the plots are closer to the theoretical value for SE, which suggests the dominance of SE for both intermediate and higher voltage of the reverse current conduction mechanism due to the "thermally-activated carriers" emitted over the M–S barrier [24]. Whereas at low voltage, it corresponds to PFE in which the defect states govern the conduction [25].

3.2. Capacitance–Voltage (C–V) Characteristics

The *C*–*V* measurement is done at a very high frequency (1 MHz). The *C*–*V* measurement has been analyzed using the depletion capacitance equation for SBDs as follows [26]:

$$\frac{1}{C^2} = \frac{2}{A^2 q\varepsilon_0\varepsilon_r N_D}\left(V_i - \frac{kT}{q} - V\right), \quad (20)$$

and the φ_B is given as

$$\varphi_B = V_i + \frac{kT}{q}\ln\frac{N_C}{N_D}. \quad (21)$$

The calculated value of barrier height from the plot between $1/C^2$ vs. the applied voltage (Fig. 11) is 0.727 eV, and donor concentration (N_D) is 8.97×10^{14} cm^{-3}.

The φ_B values are smaller by *I*–*V* technique as compared to *C*–*V* technique. These lower values obtained by *I*–*V* technique because of the presence of the native oxide layer at the M–S interface [27–30]. Any damage at the M–S interface alters the *I*–*V* characteristics because defects may act as recombination centers or as traps for trap-assisted tunnel currents. *C*–*V* measurements are not affected by such defects since interfacial capacitance and capacitance due to the depletion layer are in series. As *I*–*V* techniques involve the flow of electrons from semiconductor to metal, the φ_B obtained from this method will give lower value than from *C*–*V* measurements. These smaller values by *I*–*V* technique may be due to presence of lateral inhomogeneities in the Schottky barrier height (SBH) at the Ni/*n*-GaN interface [31, 32], the influence of image-force and dipole lowering effects, and may be due to the tunneling and leakage currents [33, 34].

Table 3. The theoretical and the experimental values of Poole–Frenkel emission and Schottky emission of Ni/*n*-GaN SBD's

Poole–Frenkel emission (10^{-3} V/cm)$^{-1/2}$		Schottky emission (10^{-3} V/cm)$^{-1/2}$	
theoretical	experimental	theoretical	experimental
9.51	1.22	4.75	1.14

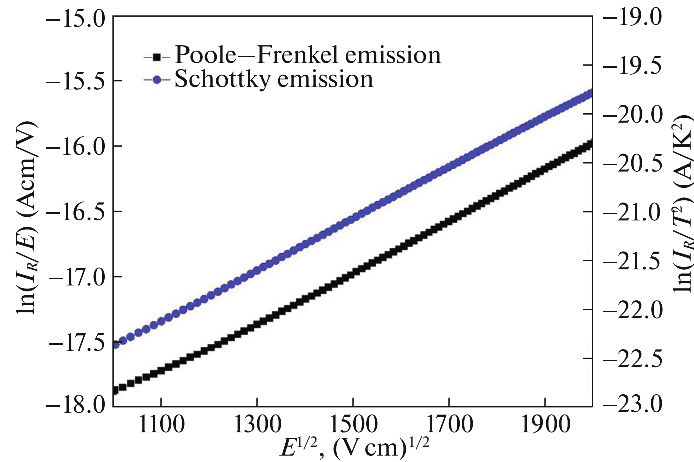

Fig. 10. The plots of Poole−Frenkel emission [ln(I_R/E) vs. $E^{1/2}$] and Schottky emission [ln(I_R/T^2) vs. $E^{1/2}$] for Ni/n-GaN SBDs.

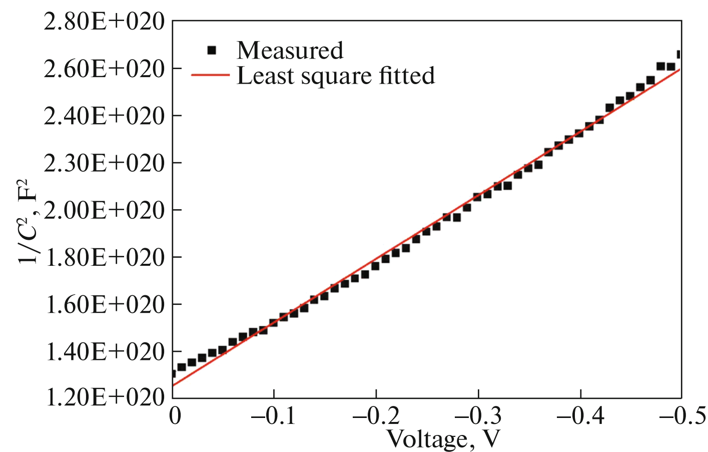

Fig. 11. The plot of $1/C^2$ vs. V for the Ni/n-GaN SBDs.

4. CONCLUSIONS

The fabrication and current transport properties of Ni/n-GaN SBDs have been discussed in the present study. The different electrical parameters have been obtained from Rhoderick's method, Cheung's method, Modified Norde's method, Hernandez's method, and Chattopadhyay method. The value of the ideality factor n extracted by Cheung's method and Chattopadhyay method is close to 1, whereas this value is approximately 2 by Rhoderick's method and Hernandez's method. It was found that the values of the barrier height φ_B obtained from the forward bias by applying different methods were nearly equal to each other, whereas the values of the series resistance R_S obtained from Cheung's and Norde methods were showing small variation with each other. Furthermore, the values of n, R_S, and φ_B obtained from different methods are compared with each other. The various methods discussed in the present study give approximately the same values of electrical parameters, which reflect the reliability of different methods for the analysis of Ni/n-GaN SBDs. The φ_B values obtained from the I–V technique (0.697 eV) are smaller than the values obtained from the C–V technique (0.727 eV), which may be due to the presence of "lateral inhomogeneities" at the Ni/n-GaN interface and "image force due to current flow across the barrier". Further, reverse current transport mechanism is mainly due to SE for intermediate and higher voltage regions. This is further verified by the forward conduction mechanism of the Ni/n-GaN SBDs.

ACKNOWLEDGMENTS

The authors are grateful for the advice and assistance of Dr. R.N. Srinivas, Department of Physics, MNIT Jaipur, and Dr. K. Asokan, IUAC, New Delhi, concerned with Schottky diodes fabrication and electrical characterization of the Schottky diodes.

CONFLICT OF INTEREST

The authors declare that they have no conflict of interest.

REFERENCES

1. L. M. Tolbert, B. Ozpineci, S. K. Islam, and M. S. Chinthavali, Semiconductors **1**, 3 (2003).
2. S. J. Pearton and C. Kuo, MRS Bull. **22** (2), 17 (1997).
3. A. C. Schmitz, A. T. Ping, M. A. Khan, Q. Chen, J. W. Yang, and I. Adesida, Semicond. Sci. Technol. **11**, 1464 (1996).
4. M. L. Gardner, *Master's Thesis* (Naval Postgraduate School, Monterey, USA, 2016).
5. T. I. Kim, Y. H. Jung, J. Song, D. Kim, Y. Li, H. Kim, S. Song, J. J. Wierer, H. Pao, Y. Huang, and J. A. Rogers, Small **8**, 1643 (2012).
6. Q. Zheng, C. Li, A. Rai, J. H. Leach, D. A. Broido, and D. G. Cahill, Phys. Rev. Mater. **3**, 014601 (2019).
7. Y. Chen, Z. Zhang, H. Jiang, Z. Li, G. Miao, H. Song, H. Liqin, and T. Guo, Nanoscale **11**, 1351 (2019).
8. E. H. Rhoderick and R. H. Williams, *Metal–Semiconductor Contacts*, 2nd ed. (Clarendon, Oxford, 1988), p. 54.
9. S. K. Cheung and N. W. Cheung, Appl. Phys. Lett. **49**, 85 (1986).
10. H. Norde, J. Appl. Phys. **50**, 5052 (1979).
11. R. T. Tung, Mater. Sci. Eng. R **35**, 1 (2001).
12. M. P. Hernández, C. F. Alonso, and J. L. Pena, J. Phys. D: Appl. Phys. **34**, 1157 (2001).
13. S. Chattopadhyay, L. K. Bera, S. K. Ray, P. K. Bose, and C. K. Maiti, Thin Solid Films **335**, 142 (1998).
14. H. C. Card and E. H. Rhoderick, J. Phys. D: Appl. Phys. **4**, 1589 (1971).
15. A. R. Arehart, B. Moran, J. S. Speck, U. K. Mishra, S. P. Ben Baars, and S. A. Ringel, J. Appl. Phys. **100**, 023709 (2016).
16. H. Kim, M. Schuette, H. Jung, J. Song, J. Lee, W. Lu, and J. C. Mabon, Appl. Phys. Lett. **89**, 053516 (2006).
17. S. Y. Karpov, D. A. Zakheim, W. V. Lundin, A. V. Sakharov, E. E. Zavarin, P. N. Burnkov, E. Y. Lundina, and A. F. Tsatsulnikov, Semicond. Sci. Technol. **33**, 025009 (2018).
18. P. F. Ruths, S. Ashok, S. J. Fonash, and D. J. M. Ruths, IEEE Trans. Electron Dev. **28**, 1003 (1981).
19. A. Kumar, S. Vinayak, and R. Singh, in *Proceedings of the Symposium on Semiconductor Materials and Devices Semiconductors, Vadodara, 2011*, J. Nano-Electron. Phys. **3**, 671 (2011).
20. Y. S. Ocak, M. Kulakci, T. Kılıçoğlu, R. Turan, and K. Akkılıç, Synth. Met. **159**, 1603 (2009).
21. V. R. Reddy, V. Janardhanam, C. H. Leem, and C. J. Choi, Superlatt. Microstruct. **67**, 242 (2014).
22. R. D. Gould and T. S. Shafai, Thin Solid Films **373**, 89 (2000).
23. C. H. Han and K. Kim, IEEE Electron Dev. Lett. **12**, 74 (1991).
24. D. K. Schroder, *Semiconductor Material and Device Characterization*, 3rd ed. (Wiley, Hoboken, 2006), p. 89.
25. J. Lin, S. Banerjee, J. Lee, and C. Teng, Electron Dev. Lett. **11**, 191 (1990).
26. T. S. Shafai and T. D. Anthopoulos, Thin Solid Films **398**, 361 (2001).
27. S. Altındal, S. Karadeniz, N. Tuğluoğlu, and A. Tataroğlu, Solid-State Electron. **47**, 1847 (2003).
28. V. R. Reddy, B. Asha, and C. J. Choi, J. Semicond. **38**, 064001 (2017).
29. Y. P. Song, R. L. V. Meirhaeghe, W. H. Laflere, and F. Cardon, Solid-State Electron. **29**, 633 (1986).
30. J. H. Werner and H. H. Güttler, J. Appl. Phys. **69**, 1522 (1991).
31. B. Boyarbay, H. Cetin, M. Kaya, and E. Ayyildiz, Microelectron. Eng. **85**, 721 (2008).
32. C. Fontaine, T. Okumura, and K. N. Tu, J. Appl. Phys. **54**, 1404 (1983).
33. R. Padma, G. Nagaraju, V. R. Reddy, and C. J. Choi, Thin Solid Films **598**, 236 (2016).
34. L. Geng, F. A. Ponce, S. Tanaka, and Y. Nakagawa, Phys. Status Solidi A **188**, 803 (2001).

View publication stats